Available online at www.sciencedirect.com

ScienceDirect

Acta Materialia 92 (2015) 55–63

Acta MATERIALIA

www.elsevier.com/locate/actamat

Origin of shear induced β to ω transition in Ti–Nb-based alloys

M.J. Lai, C.C. Tasan,* J. Zhang, B. Grabowski, L.F. Huang and D. Raabe

Max-Planck-Institut für Eisenforschung GmbH, Max-Planck-Straße 1, 40237 Düsseldorf, Germany

Received 24 October 2014; accepted 22 March 2015

Abstract—Ti–Nb-based alloys are essential materials for biomedical implant and aerospace applications. They reveal complex phase transformation behavior. Here, a $\{2\,1\,1\}_\beta\langle 1\,1\,1\rangle_\beta$ twinning induced β (body-centered cubic phase) to ω (hexagonal phase) transition in Ti–Nb-based alloys is demonstrated by transmission electron microscopy and analyzed employing *ab initio* calculations and the linear elastic inclusion theory. Our theoretical results reveal a distinct energy barrier for the β to ω transition, where the contribution from lattice rearrangement, rather than the elastic contribution associated with lattice parameter mismatch, plays the major role. It is shown that this energy barrier can be overcome by $\{2\,1\,1\}_\beta\langle 1\,1\,1\rangle_\beta$ shear, explaining why $\{2\,1\,1\}_\beta\langle 1\,1\,1\rangle_\beta$ twinning or, alternatively, the β to α″ (orthorhombic phase) transition promotes local formation of the ω phase.

Keywords: Titanium; *Ab initio*; ω phase; TEM; Phase transformation

1. Introduction

Allotropic transformations between the high-temperature body-centered cubic (bcc) β phase and the lower-temperature hexagonal close-packed (hcp) α phase exist in group IV elements such as Ti, Zr and Hf. Upon alloying with β-stabilizing elements such as V, Mo, Nb, W or Ta the resultant alloys may form a number of other stable or metastable phases including hcp α′, base-centered orthorhombic α″, non-close-packed hexagonal ω and some intermetallic phases. Improved understanding of the metastable ω phase in β-type Ti alloys and Zr alloys is of high relevance since its discovery, due to its roles in affecting mechanical and physical properties and its special formation mechanism [1]. Banerjee et al. [2] documented the various ω phase morphologies and underlying formation mechanisms: The β to ω transformation can occur (i) thermally, i.e., via rapid cooling from the single bcc β phase field or by subsequent isothermal aging, producing ellipsoidal or cuboidal ω particles homogeneously distributed throughout the β matrix; or (ii) mechanically, i.e., via extremely high strain-rate compressive loading (shock loading), producing non-uniformly distributed ω plates (hereafter referred to as plate-like ω) [3,4].

Interestingly, recent studies on Ti–Nb-based alloys [5–7] report about a similar plate-like ω phase during quasi-static compression (in the vicinity of the $\{2\,1\,1\}_\beta\langle 1\,1\,1\rangle_\beta$ twin boundary, see Fig. 3 in Ref. [6]) and even during quenching (at the α″/β interface, see Fig. 2 in Ref. [7]) as listed in Table 1. Considering that, both twinning and α″ transformation involve a shear process [8], it can be assumed that the formation of the plate-like ω phase is due to the local atomic shear rather than to the macroscopic compressive stress state. This assumption, however, is so far not fully confirmed in the literature. Moreover, for the compositions listed in Table 1 (valence electron number $e/a = 4.22$–4.24), previous *ab initio* investigations [9,10] show that the ω phase is energetically more stable compared to the β phase, anticipating a spontaneous transition from β to ω, in contrast to the experimentally observed requirement for shear-assistance. Taking into account that the formation of an ω inclusion is associated with a lattice mismatch [11] and that the phase transformation is a kinetic process, it can be assumed that the atomic shear primarily follows one of the two principles, namely, decreasing the elastic strain energy associated with lattice mismatch between β and ω, or overcoming a kinetic barrier associated with the energetic pathway. This is another aspect that is not fully clarified yet.

The present work thus aims at providing an improved understanding on these two points. First, for addressing the former aspect, we performed both cold rolling and uniaxial tension experiments on a Ti–Nb-based alloy with a valence electron number value e/a in the same range and then examined whether the $\{2\,1\,1\}_\beta\langle 1\,1\,1\rangle_\beta$ twin introduced by the two different loading modes induces similar plate-like ω phases along the twin boundary. For the latter aspect, a treatise based on *ab initio* calculations and the theory of elastic inclusion was carried out to clarify the full energetic context of the atomic shear.

* Corresponding author.

http://dx.doi.org/10.1016/j.actamat.2015.03.040
1359-6462/

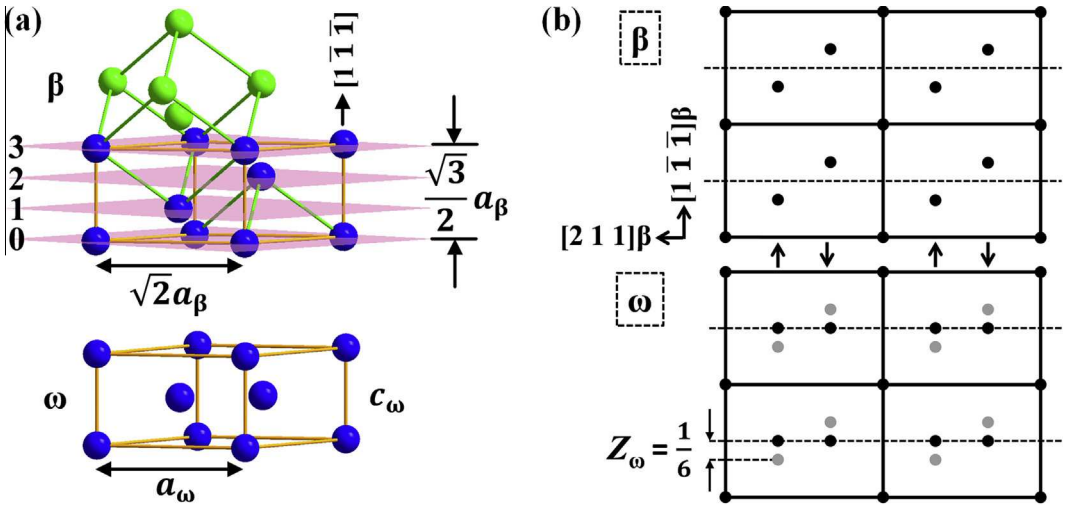

Fig. 1. Relationship between bcc β and hexagonal ω structures. (a) Hexagonally illustrated β and ω crystal lattices. (b) $(0\bar{1}1)_\beta//(1\bar{2}10)_\omega$ atomic plane showing a shuffle transformation process from β to ω.

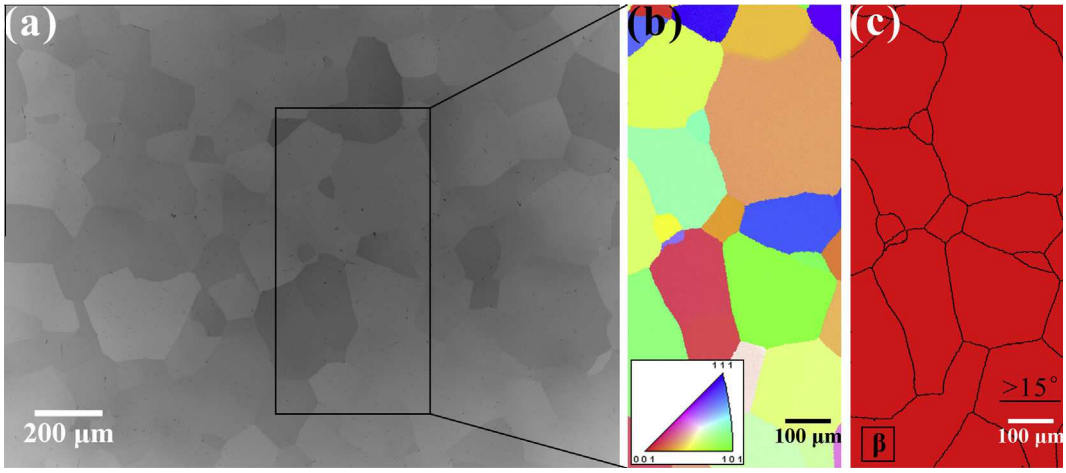

Fig. 2. Microstructure of the as-homogenized Ti–36Nb–1.4Ta–2.8Zr–0.3O alloy: (a) BSE image; (b) EBSD inverse pole figure map; (c) EBSD phase map of the bcc β phase, where the grain boundaries (>15°) are also shown.

2. Experimental procedure

For the experiments, we used a laboratory-cast Ti–36Nb–1.4Ta–2.8Zr–0.3O (wt.%, $e/a = 4.23$) ingot. It was melted in an arc-melting furnace under argon atmosphere and cast into a copper mold. The as-cast material was then homogenized at 1200 °C for 4 h, under vacuum, followed by furnace cooling. Individual samples were cut from the ingot using electron discharge machining. The initial microstructure was characterized by backscattered electron (BSE) imaging and electron backscatter diffraction (EBSD) mapping using a Zeiss-Crossbeam XB 1540 FIB-SEM instrument (Carl Zeiss SMT AG, Germany) at an accelerating voltage of 15 kV. A plate with a thickness of 5 mm was subjected to 3.5% rolling at room temperature. To examine the situation of tensile loading, uniaxial tension was conducted to a sheet of 10 mm × 1 mm cross section until fracture. Disks of 3 mm diameter were cut (close to the fracture surface in the case of uniaxial tension) and then mechanically thinned to less than 100 μm followed by twin-jet electro-polishing until perforation. The electro-polishing was performed at 6 °C and 20 V in an electrolyte of 60 ml perchloric acid, 350 ml butoxyethanol and 590 ml methanol. Transmission electron microscopy (TEM) observations were carried out on a JEOL JEM-2200FS microscope operated at 200 kV.

3. Simulation methodology

Generally, the ω phase forms by a $\{1\bar{1}\bar{1}\}_\beta$ collapse mechanism or, equivalently, by atomic shuffling on a $\{2\,1\,1\}_\beta$ plane along a $<1\bar{1}\bar{1}>_\beta$ direction [1,2] as shown in Fig. 1(a) and (b), respectively: 2/3 of the atoms in the $\{1\bar{1}\bar{1}\}_\beta$ layers (layer "1" and layer "2") collapse to a middle plane between them with the third layer left unaltered. Fig. 1(a) shows that both the β phase (with lattice parameter a_β) and ω phase (with lattice parameter a_ω and c_ω) can be depicted by a hexagonal lattice with three atoms per unit cell, giving the lattice parameter correspondence between a_ω, c_ω and $\sqrt{2}a_\beta$, $\sqrt{3}a_\beta/2$, respectively. The atomic

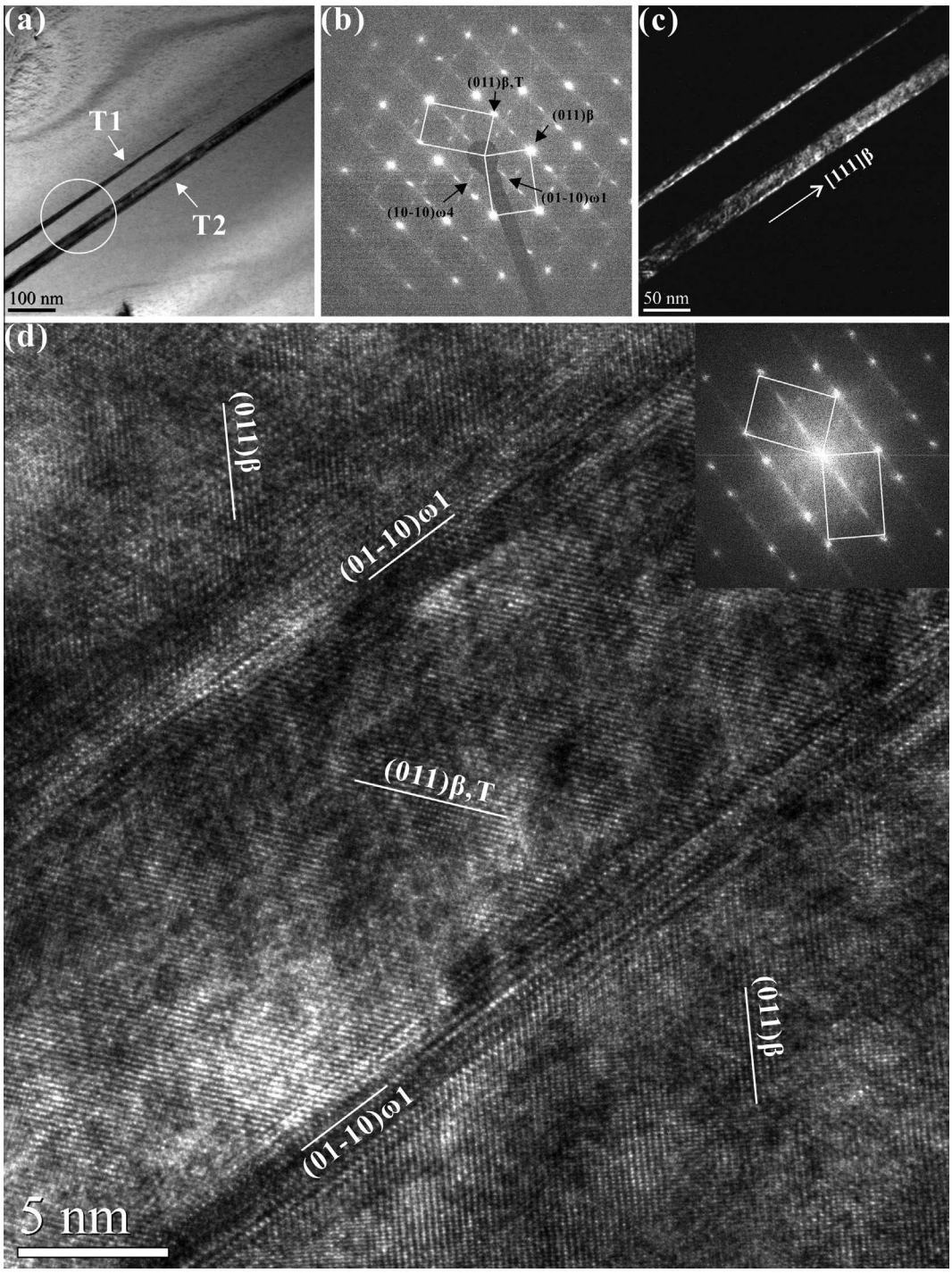

Fig. 3. TEM images of the 3.5% cold rolled sample. (a) Bright field image displaying two twin lamellae (referred to as T1 and T2). (b) $[0\bar{1}1]_{\beta}$ selected area diffraction pattern of the circled area in (a). $(2\bar{1}\bar{1})_{\beta}[1\,1\,1]_{\beta}$ twin and two variants of ω are illustrated. (c) Dark field image taken using the twin reflection $(0\,1\,1)_{\beta,T}$. (d) HRTEM image of T1, where the inset shows its FFT image corresponding to the electron diffraction pattern.

positions are $(0,0,0)$, $(2/3,1/3,2/3-Z_{\omega})$ and $(1/3,2/3,1/3+Z_{\omega})$ with the latter two atoms belonging to the same sub-lattice, where $Z_{\omega}=0$ defines the bcc β crystal, $0<Z_{\omega}<1/6$ defines the non-ideal ω crystal and $Z_{\omega}=1/6$ defines the ideal ω crystal. The $\beta\rightarrow\omega$ transformation strain tensor can be expressed as

$$\varepsilon_{ij}^{0}=\frac{1}{3}\begin{bmatrix}2\eta_1+\eta_2 & \eta_1-\eta_2 & \eta_1-\eta_2\\ \eta_1-\eta_2 & 2\eta_1+\eta_2 & \eta_2-\eta_1\\ \eta_1-\eta_2 & \eta_2-\eta_1 & 2\eta_1+\eta_2\end{bmatrix}, \tag{1}$$

where $\eta_1=a_{\omega}/(\sqrt{2}a_{\beta})-1$ and $\eta_2=2c_{\omega}/(\sqrt{3}a_{\beta})-1$. The corresponding elastic strain energy in a stress-free state was calculated using the Khachaturyan theory for an elastic inclusion [12,13]:

$$\Delta F^{\mathrm{els}}=\frac{1}{2}\int\int\int B(\boldsymbol{e})|\theta(\boldsymbol{k})|^2\,\frac{d^3k}{(2\pi)^3} \tag{2}$$

where $\theta(\boldsymbol{k})$ is the Fourier transform of the shape function of the inclusion, and

Table 1. Composition, valence electron number e/a, processing state of Ti–Nb-based alloys that show a plate-like ω phase. The corresponding microstructural location of the ω phase is also listed.

Composition	e/a	Processing state	Location of ω phase
Ti–23Nb–0.7Ta–2Zr–1.2O (at.%) [6]	4.24	Compression	$\{2\,1\,1\}_\beta\langle 1\,1\,1\rangle_\beta$ twin boundary
Ti–35.7Nb–2.01Ta–2.98Zr (wt.%) [5]	4.24	Quenching	α″/β interface
Ti–22Nb (at.%) [7]	4.22	Quenching	α″/β interface
Ti–24Nb (at.%) [7]	4.24	Quenching	α″/β interface

$$B(\boldsymbol{e}) = \lambda_{ijkl}\varepsilon^0_{ij}\varepsilon^0_{kl} - e_i\sigma^0_{ij}\Omega_{jl}(\boldsymbol{e})\sigma^0_{lm}e_m \quad (3)$$

is a function of the direction $\boldsymbol{e} = \boldsymbol{k}/k$. λ is the elastic constant tensor, which correlates the transformation stress with strain according to Hooke's law, $\sigma^0_{ij} = \lambda_{ijkl}\varepsilon^0_{kl}$, and Ω a Green's tensor defined by its inverse $\Omega^{-1}_{ij}(\boldsymbol{e}) = \lambda_{iklj}e_k e_l$. In this work, the difference between the moduli of β and ω of the same composition was neglected. This approximation is justified due to the composition invariance and the crystallographical match of the β and ω lattices.

The chemical contribution to the total free energy at a Wigner–Seitz radius r and temperature T can be approximated as $F^{\text{chem}}(r, T) = E(r) + F_{\text{vib}}(r, T) + F_{\text{elec}}(r, T)$, where E is the 0 K total energy, F_{vib} the phonon vibrational free energy calculated by the Debye–Grüneisen model [14,15] and F_{elec} the thermal electronic contribution to the free energy [16]. The details for the calculation of F_{vib} and F_{elec} are presented as Supplementary Online Material. The 0 K total energy was calculated using the exact muffin-tin orbitals (EMTO) method [17–19], where the chemical disorder was treated by coherent potential approximation [20,21]. The one-electron equations were solved within the scalar-relativistic and soft-core approximations. The EMTO self-consistent calculations were performed for a muffin-tin basis set including s, p, d, f orbitals, and the Green function for the valence states was calculated for 60 complex energy points exponentially distributed on a semicircular contour with 2.8–3.6 Ry diameter enclosing the occupied states. The elastic constants of the bcc structure (β phase) were calculated using the volume-conserving orthorhombic and monoclinic distortion method [19] for six distortions $\varepsilon = 0.00, 0.01, \ldots, 0.05$. The k-point meshes were carefully tested such that 3549–19683 uniformly distributed k-points were used to sample the irreducible wedge of the Brillouin zones depending on the crystal structures and distortions. The Perdew–Burke–Ernzerhof functional in generalized gradient approximation is used to describe the electronic exchange and correlation [22].

4. Results and discussion

4.1. Twinning induced β to ω transformation

The typical microstructure of the as-homogenized Ti–36Nb–1.4Ta–2.8Zr–0.3O (wt.%) alloy is shown in Fig. 1. The alloy presents an equiaxed microstructure consisting of β grains with about 80 μm size. Neither BSE nor EBSD detected any twins in the pre-deformed alloy. The absence of twins is also confirmed by TEM observations reported in a previous work [23]. It should be noted that small amounts of granular ω phases formed during the final cooling were observed by TEM. The relatively small size (less than 10 nm) and limited volume fraction of the ω particles render them invisible to the spatial resolution of BSE and EBSD.

After 3.5% cold rolling, twin lamellae with nano-scale width were found in the alloy as displayed in Fig. 3. The bright-field image in Fig. 3(a) shows two twin lamellae (referred to as T1 and T2) oriented along the $[1\,1\,1]_\beta$ direction. The width of T1 and T2 is 12 nm and 27 nm, respectively, while their length extends over several microns. The $[0\,\bar{1}\,1]_\beta$-zone selected area diffraction (SAD) pattern (Fig. 3(b)) and dark-field image (Fig. 3(c)) of these two lamellae indicate that they are $(2\,\bar{1}\,\bar{1})_\beta[1\,1\,1]_\beta$ twins. In addition to the twin reflections, ω diffraction spots located at 1/3 and 2/3 $\{2\,1\,1\}_\beta$ positions can also be seen in Fig. 3(b). There are four variants of the ω phase with $[-2\,1\,1\,0]_{\omega1}$, $[-1\,0\,1\,4]_{\omega2}$, $[0\,1\,-1\,4]_{\omega3}$ and $[-1\,2\,-1\,0]_{\omega4}$ parallel to $[0\,\bar{1}\,1]_\beta$, where the diffraction spots of ω2 and ω3 are completely overlapping with those of the β phase. Thus, only ω1 and ω4 are distinguishable in the SAD pattern. Since the four ω variants formed with equal probability during the cooling process following homogenization [1,23], the populations of them are equal and, hence, it is reasonable to observe both ω1 and ω4 spots in Fig. 3(b). Interestingly, a difference in diffraction intensity between these two variants is observed as well, where ω1 shows higher intensity, indicating that more ω1 formed during the cold rolling.

High resolution transmission electron microscopy (HRTEM) images reveal that there is a layer of the ω phase along the boundary between the $(2\,\bar{1}\,\bar{1})_\beta[1\,1\,1]_\beta$ twin and the β matrix. As an example, Fig. 3(d) displays the HRTEM image of T1, where the inset is its Fourier filtered transformation (FFT) image corresponding to the electron diffraction pattern. The plate-like ω phase located along the twin boundary is indexed as ω1 variant, whose diffraction intensity is much higher than that of the other variant ω4 as seen in the FFT image. The orientation relationship between the β matrix and the plate-like ω phase is $(-2\,1\,1)_\beta//(0\,1\,-1\,0)_\omega$. Apparently, the additional formation of the plate-like ω phase leads to the higher diffraction intensity of the ω1 variant.

In the case of uniaxial tension, identical phenomenon concerning $\{2\,1\,1\}_\beta\langle 1\,1\,1\rangle_\beta$ twinning and plate-like ω phase is observed, as shown in Fig. 4. Fig. 4(a) is a TEM bright field image showing a $(2\,1\,1)_\beta[\bar{1}\,1\,1]_\beta$ twin lamella in the alloy deformed by uniaxial tension. The diffraction pattern and its key diagram, Fig. 4(b), illustrate that the twinned β reflections overlap the matrix and the ω reflections, rendering corresponding ω diffraction spots brighter. The HRTEM image in Fig. 4(c) reveals ω phase regions aligned along the twin boundary in the same manner as found for the cold rolling and compression cases [6]. This demonstrates that the formation of plate-like ω phase accompanying $\{2\,1\,1\}_\beta\langle 1\,1\,1\rangle_\beta$ twinning is not exclusive to the macroscopic compressive stress state. It depends on twinning itself, rather than on the specific loading mode.

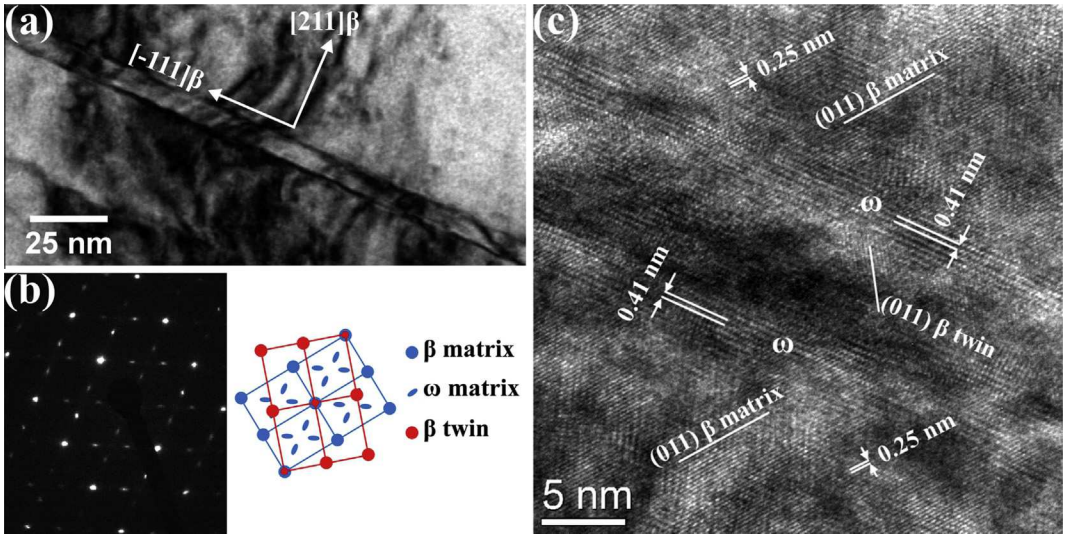

Fig. 4. (a) TEM bright field image showing a twin lamella in the sample deformed by uniaxial tension; (b) $[0\,1\,\bar{1}]_{\beta}$ selected area diffraction pattern with corresponding key diagram and (c) high resolution TEM image of the twinned area revealed in (a).

Since small amounts of ω particles were already present in the as-homogenized microstructure, it is important to clarify if the plate-like ω phase is formed by a preferential growth of the pre-existed ω particle or by nucleation of a new twinning-induced ω phase. During deformation the local stress state may affect the equally-probable growth of the four ω variants, promoting selective growth of a specific variant and inhibiting the growth of others. This assumption is nonetheless excluded by taking into account the low temperature and the limited dwell time of the deformation processes. In general, the growth of the ω phase in β titanium alloys occurs at 150–500 °C and the process is known to be sluggish [24–27]. For example, the ω particles with an average size <10 nm in Ti-9 at.% Mo alloy require 48 h at 475 °C to grow to an average size of ~40 nm [24]. Here, the plate-like ω phase extends to several microns accompanying the $\{2\,1\,1\}_{\beta}\langle 1\,1\,1\rangle_{\beta}$ twin, but the dwell time of the deformation processes is less than one minute, which is apparently not enough for the nano-sized particles to grow to a plate with a length of several microns. On the other hand, the formation of plate-like ω phase along the $\{2\,1\,1\}_{\beta}\langle 1\,1\,1\rangle_{\beta}$ twin boundary in the similar composition without pre-existed ω phase [6] already proves that the ω plate is newly nucleated, i.e., induced by twinning.

The ω particles already present prior to deformation may act as barriers for dislocation slip [28,29], but they seem to play a minor role in the propagation of twin. This situation is also true for the $\{3\,3\,2\}_{\beta}\langle 1\,1\,3\rangle_{\beta}$ twin occurred in metastable β titanium alloys [30,31].

4.2. Elastic and chemical contributions to the relative phase stability between β and ω

The governing potential of the β to ω transformation for a specific composition is the total free energy difference, which concerns the elastic contribution associated with lattice parameter mismatch and the chemical contribution from lattice rearrangement (Fig. 1(a)). Previous studies [9,10] considering only the chemical contribution at 0 K predict a spontaneous transformation from β to ω. Nonetheless, as shown in the previous subsection, the plate-like ω phase formed inside the bulk β matrix and linked to the bcc β lattice coherently, may introduce elastic strain energy to the system if there is a lattice parameter mismatch between these two phases. On the other hand, temperature effects may also contribute to the relative stability of β and ω.

To our knowledge, few studies exist on the measurement of the lattice parameter of the ω phase in Ti–Nb-based alloys due to the difficulty associated with its relatively small size and limited volume fraction. In this work, *ab initio* simulations were used to assess the room-temperature lattice parameters of β and ω phases of Ti–Nb alloys with temperature effects approximated by the Debye–Grüneisen model [14,15]. Fig. 5(a) and (b) presents the lattice parameters of the β and ω phases of Ti–Nb alloys ($e/a = 4.14$–4.30), respectively. Available experimental data [32–34] are also displayed for comparison. A good agreement between theory and experiment is shown and the experimentally observed slightly increasing trend in a_{β} is well reproduced. For a specific composition, the volume per atom of the ω phase turns out to be larger than that of the β phase (not shown here), similar to the volume expansion phenomena in Ti–V alloys observed via neutron diffraction [11]. When β transforms to ω, there is an enlargement in $a_{\langle 110\rangle\beta}$ ($\sqrt{2}a_{\beta}$) and a decrease in $a_{<1\,\bar{1}\,\bar{1}>_{\beta}}$ ($\sqrt{3}a_{\beta}/2$), and, therefore, a homogeneous isotropic strain in the $\{1\,1\,1\}_{\beta}$ planes and a change in the spacing between adjacent $\{1\,1\,1\}_{\beta}$ planes are induced. Thus, these lattice parameter differences cause a lattice mismatch between ω and the surrounding β, hence introducing an elastic misfit strain into the system.

Fig. 6(a) displays the elastic strain energy ΔF^{els} of the plate-like ω inclusion formed inside the β matrix which was calculated based on the experimentally determined habit plane $\{2\,1\,1\}_{\beta}$ [6] and theoretical structural parameters, assuming an infinitesimal thickness of the ω plate. For comparison, the $\Delta F^{\mathrm{els}}_{\mathrm{exp}}$ calculated with the lattice parameters and elastic constants of the β phase interpolated and extrapolated from the available experimental data [33,35,36] are also shown. Both sets of elastic strain energies increase with e/a, which can be interpreted by the

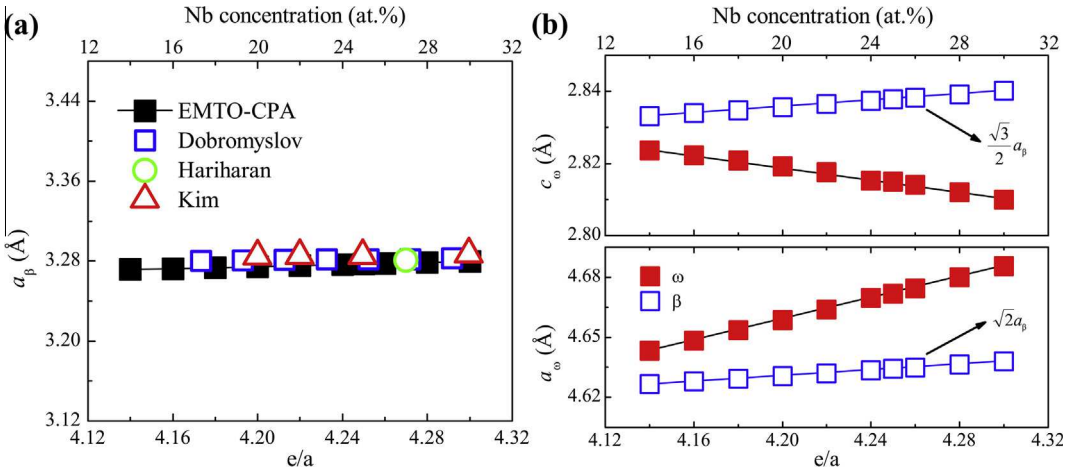

Fig. 5. Lattice parameters of the β and ω phases of Ti–Nb alloys at room temperature. (a) Theoretically predicated lattice parameters of the β phase compared with available experimental data [32–34]. (b) Theoretically predicted lattice parameters of the ω phase compared with those of the β phase.

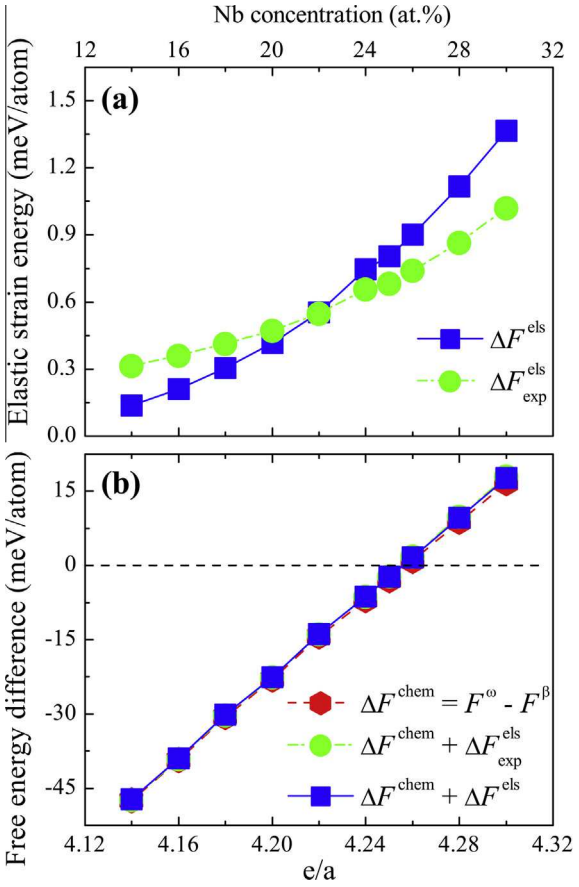

Fig. 6. Elastic and chemical contributions to the free energy difference between the β and ω phases as a function of *e/a* in the Ti–Nb alloys. (a) Elastic strain energy ΔF^{els} determined by *ab initio* simulations. For comparison, the ΔF^{els}_{exp} determined based on the experimental structural parameters of β phase [33,35,36] is also included. (b) Chemical free energy ΔF^{chem} associated with lattice rearrangement from β to ω. The combination of elastic and chemical contributions is also shown.

enhancing mismatch between the lattice parameters of β and ω phases (Fig. 5(b)).

In order to clarify whether the elastic contribution to the total free energy opposes a spontaneous transformation from β to ω, the chemical contribution at room temperature is calculated as $\Delta F^{chem} = F^{\omega} - F^{\beta}$ with F^{ω} and F^{β} being the chemical free energies of the ω and β phases, respectively. Fig. 6(b) shows ΔF^{chem} as a function of *e/a* (Nb concentration), revealing that ΔF^{chem} increases monotonically with increasing Nb concentration, reproducing the experimentally determined β-stabilizing effect of Nb. Similar to Ref. [9,10], the ω phase appears to be thermodynamically more stable than the β phase in the composition range of $e/a = 4.22$–4.25 even when the temperature effect is taken into account.

Although the elastic contribution favors the β phase, for $e/a = 4.22$–4.25 it is too small to compete with the energy difference determined by the chemical contribution ΔF^{chem}. As seen in Fig. 6(b), the combination of elastic and chemical contributions still shows an energy gap between β and ω for $e/a = 4.22$–4.25, indicating the existence of a thermodynamic driving force for a spontaneous transition from β to ω. This result contradicts current experimental observations of a shear assisted transformation [5–7].

4.3. Energy barrier of the β to ω transformation

As discussed above, when only comparing the free energies of β and ω, the β to ω transition is expected to occur spontaneously even when the elastic contribution and temperature effects are taken into account. In fact, such a comparison ignores the energy change of the intermediate transition states ($0 < Z_\omega < 1/6$) transiently formed during the transformation process. If the transformation (from $Z_\omega = 0$ to $Z_\omega = 1/6$) is spontaneous, the energy of these intermediate transition states should decrease monotonously with the increase of Z_ω. In order to probe the energy landscape along the transformation path, *ab initio* calculations were performed to determine the chemical free energies of seven intermediate transition states with $Z_\omega = 1/48,\ 2/48,\ldots,\ 7/48$ between the β and ω structures. During the calculations, the lattice parameters of each crystal structure were optimized to minimize the total energy. Taking Ti-24Nb alloy ($e/a = 4.24$) as an example, the change of the chemical energies ΔF^{chem} with respect to the β structure for each intermediate structure is shown in

Fig. 7, where the inset illustrates the $(0\bar{1}1)_\beta$ and $(1\bar{2}10)_\omega$ atomic planes characteristic of the movement of the inner two atoms (i.e., transformation path). When the inner atoms move from the positions they occupy in the β phase to their new positions in the ω phase (see Supplementary Movie which also shows the change of the lattice parameters), ΔF^{chem} increases first up to a maximum near $Z_\omega = 3/48$, and then decreases monotonously until the transition is finished. This result reveals an energy barrier of ~6.04 meV/atom for the transformation pathway. Based on the theoretically determined structural parameters, the elastic strain energy ΔF^{els} of each intermediate transition state was calculated as well. The elastic contribution slightly enlarges the energy barrier to ~6.30 meV/atom, but contributes only 4% to the total barrier value. Our results also demonstrate that the energy barrier is composition dependent and drops with the decrease of *e/a*. When the *e/a* is 4.14, the energy barrier falls to ~1.87 meV/atom (including the elastic contribution). The existence of the energy barrier suggests that the β to ω transformation in the above experimentally investigated composition range (*e/a* = 4.22–4.24) is not spontaneous and, hence, requires the contribution of external stimuli.

To this end, thermal fluctuations at around room temperature are not sufficient, although a simple comparison of the energy barrier and the mean kinetic energy (~26 meV/atom for room temperature) seems suggestive of a thermally driven transition. Such a scenario is, however, ruled out by taking into account the fact that the transition process requires a highly correlated atomic movement of a sufficiently large nucleus to form the first instance of the ω phase. The corresponding probability of this correlated movement to occur (i.e., the product of the individual probabilities of the atoms to perform a movement into the specific direction) is negligibly small when considering the weakly correlated thermal fluctuations. Instead, we have to extend the search to external stimuli that naturally inherit the type of correlated movement required for the phase transformation.

4.4. Role of atomic shear in overcoming the energy barrier

As displayed in Fig. 7, if there is a local stress moving a pair of adjacent $\{2\,1\,1\}_\beta$ atomic planes along the $<1\,\bar{1}\,\bar{1}>_\beta$ direction by a displacement of $Z_\omega = \pm 3/48$, the energy barrier will be overcome and then the transition can occur spontaneously. Thus, the atomic shear along the $\{2\,1\,1\}_\beta<1\,\bar{1}\,\bar{1}>_\beta$ direction can act as an assisting factor. Indeed, this explains why the $\{2\,1\,1\}_\beta<1\,\bar{1}\,\bar{1}>_\beta$ twinning or β to α″ transformation induces a plate-like ω phase in Ti–Nb-based alloys with an *e/a* range of 4.22–4.24, as schematically illustrated in Fig. 8. The bcc structure of the β phase can be generated by a stacking of $\{2\,1\,1\}_\beta$ planes. Crystallographically, the $\{2\,1\,1\}_\beta<1\,\bar{1}\,\bar{1}>_\beta$ twinning can be referred to as a consecutive shearing of $\{2\,1\,1\}_\beta$ planes along the $<1\,\bar{1}\,\bar{1}>_\beta$ direction [37], while the β to α″ transformation involves (i) shearing of atoms in the $<1\,\bar{1}\,\bar{1}>_\beta$ direction within the $\{2\,1\,1\}_\beta$ plane and (ii) shuffling of atoms in every other $0\,1\,\bar{1}_\beta$ atomic plane [8,38]. Both processes impose a $\{2\,1\,1\}_\beta<1\,\bar{1}\,\bar{1}>_\beta$ shear stress on the surrounding β matrix, which assists in overcoming the energy barrier on the β to ω transition pathway and, therefore, induces the formation of a sequence of ω phases aligned along the $\{2\,1\,1\}_\beta<1\,\bar{1}\,\bar{1}>_\beta$ twin boundary or α″/β interface.

It should be noted that the energy barrier can be overcome by thermal activation as well if the alloy is subjected to higher temperature. Normally, the ω transformation start temperature in β titanium alloys is 150–500 °C [24–27]. For the Ti–35.7Nb–2.01Ta–2.98Zr (wt.%) alloy, a similar composition as that investigated in this work, in situ synchrotron X-ray diffraction analyses indicate that the ω phase starts to form at around 200 °C [5]. This explains the existence of dispersed ω phase precipitates in the β matrix prior to deformation (Subsection 4.1), considering the long exposure to high temperature during gradual furnace cooling.

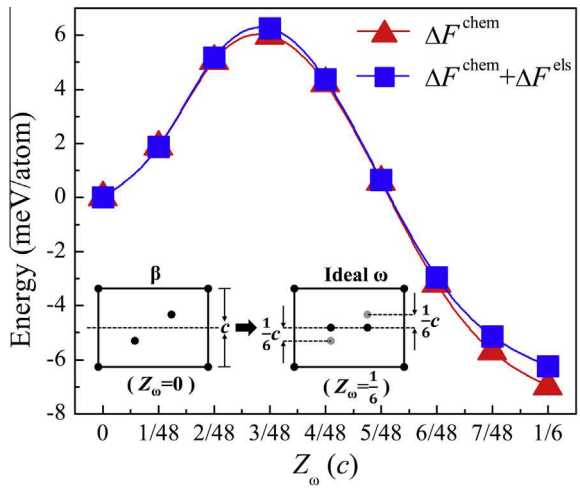

Fig. 7. Change of free energy during the β to ω transition process in Ti–24Nb alloy at room temperature. ΔF^{chem} and ΔF^{els} are the *ab initio* determined chemical and elastic contributions, respectively. The inset illustrates the start and end structures of the transition process characteristic of two inner atoms moving from $Z_\omega = 0$ to $Z_\omega = 1/6$.

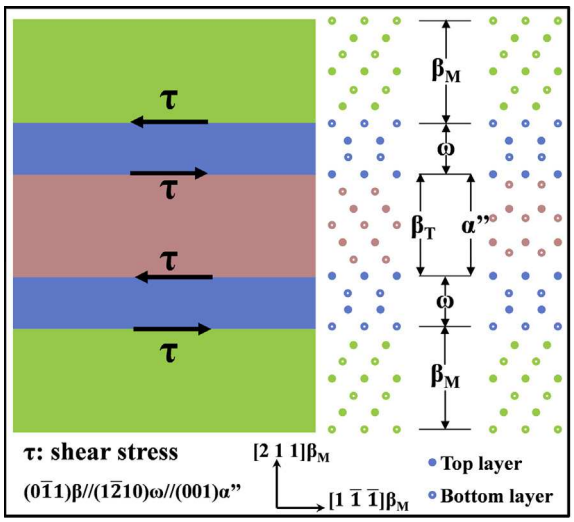

Fig. 8. Schematic representation of the formation of the plate-like ω phase induced by $\{2\,1\,1\}_\beta<1\,\bar{1}\,\bar{1}>_\beta$ twining and β to α″ phase transformation. The ω phases are located along the boundary between the β matrix (β_M) and β twin (β_T) or α″.

5. Conclusion

We explain for the first time the critical role that the $\{2\,1\,1\}_\beta\langle 1\,1\,1\rangle_\beta$ atomic shear plays for the formation of the plate-like ω phase precipitates in Ti–Nb-based alloys and reveal the theoretical background and underlying mechanisms. We draw the following conclusions:

- The formation of plate-like ω phase along the $\{2\,1\,1\}_\beta\langle 1\,1\,1\rangle_\beta$ twin boundary in Ti–Nb-based alloys with $e/a = 4.22$–4.24 is independent of the macroscopic stress state. It is induced by the $\{2\,1\,1\}_\beta\langle 1\,1\,1\rangle_\beta$ twinning.
- At room temperature, the ω phase is thermodynamically more stable than the β phase for the composition range of $e/a = 4.22$–4.25. The elastic strain energy introduced by the lattice parameter mismatch between β and ω favors the β phase, but it is too small to change the relative stability.
- There is an energy barrier on the energetic pathway of the β to ω transition, preventing a spontaneous transformation, and the $\{2\,1\,1\}_\beta\langle 1\,1\,1\rangle_\beta$ shear associated with $\{2\,1\,1\}_\beta\langle 1\,1\,1\rangle_\beta$ twinning and α″ transformation is critical in overcoming this barrier, interpreting why twin or α″ induces plate-like ω phase along their boundary.

Acknowledgments

M.J.L. would like to thank China Scholarship Council for the scholarship granted to support this work. The funding from the European Research Council under the EU's 7th Framework Programme (FP7/2007-2013)/ERC Grant Agreement No. 290998 is gratefully acknowledged.

Appendix A. Supplementary data

Supplementary data associated with this article can be found, in the online version, at http://dx.doi.org/10.1016/j.actamat.2015.03.040.

References

[1] S.K. Sikka, Y.K. Vohra, R. Chidambaram, Omega phase in materials, Prog. Mater. Sci. 27 (1982) 245.
[2] S. Banerjee, R. Tewari, G.K. Dey, Omega phase transformation – morphologies and mechanisms, Int. J. Mater. Res. 97 (2006) 963.
[3] G.K. Dey, R. Tewari, S. Banerjee, G. Jyoti, S.C. Gupta, K.D. Joshi, S.K. Sikka, A new high-pressure phase transition in a zirconium–niobium alloy, Philos. Mag. Lett. 82 (2002) 333.
[4] G.K. Dey, R. Tewari, S. Banerjee, G. Jyoti, S.C. Gupta, K.D. Joshi, S.K. Sikka, Formation of a shock deformation induced ω phase in Zr 20 Nb alloy, Acta Mater. 52 (2004) 5243.
[5] J. Zhang, C.C. Tasan, M. Lai, K. Pradeep, L. Huang, B. Grabowski, H. Springer, A. Kostka, A. Dippel, D. Raabe. (unpublished).
[6] H. Xing, J. Sun, Mechanical twinning and omega transition by <1 1 1> 1 1 2 shear in a metastable beta titanium alloy, Appl. Phys. Lett. 93 (2008) 031908.
[7] Y.W. Chai, H.Y. Kim, H. Hosoda, S. Miyazaki, Interfacial defects in Ti–Nb shape memory alloys, Acta Mater. 56 (2008) 3088.
[8] H.W. Jeong, Y.S. Yoo, Y.T. Lee, J.K. Park, Elastic softening behavior of Ti–Nb single crystal near martensitic transformation temperature, J. Appl. Phys. 108 (2010) 063515.
[9] Q.-M. Hu, S.-J. Li, Y.-L. Hao, R. Yang, B. Johansson, L. Vitos, Phase stability and elastic modulus of Ti alloys containing Nb, Zr, and/or Sn from first-principles calculations, Appl. Phys. Lett. 93 (2008) 121902.
[10] J. Sun, Q. Yao, H. Xing, W. Guo, Elastic properties of beta, alpha" and omega metastable phases in Ti–Nb alloy from first-principles, J. Phys. Condens. Matter 19 (2007) 486215.
[11] G. Aurelio, A.F. Guillermet, G.J. Cuello, J. Campo, Metastable phases in the Ti–V system: Part I. Neutron diffraction study and assessment of structural properties, Metall. Mater. Trans. A 33 (2002) 1307.
[12] A.J. Khachaturyan, Theory of structural transformations in solids, John Wiley & Sons, New York, 1983.
[13] J.W. Morris Jr., The Khachaturyan theory of elastic inclusions: recollections and results, Phil. Mag. 90 (2010) 3.
[14] V.L. Moruzzi, J.F. Janak, K. Schwarz, Calculated thermal properties of metals, Phys. Rev. B 37 (1988) 790.
[15] P. Söderlind, L. Nordström, Y. Lou, B. Johansson, Relativistic effects on the thermal expansion of the actinide elements, Phys. Rev. B 42 (1990) 4544.
[16] Y. Wang, Z.K. Liu, L.Q. Chen, Thermodynamic properties of Al, Ni, NiAl, and Ni3Al from first-principles calculations, Acta Mater. 52 (2004) 2665.
[17] L. Vitos, Total-energy method based on the exact muffin-tin orbitals theory, Phys. Rev. B 64 (2001) 014107.
[18] L. Vitos, I.A. Abrikosov, B. Johansson, Anisotropic lattice distortions in random alloys from first-principles theory, Phys. Rev. Lett. 87 (2001) 156401.
[19] L. Vitos, Computational quantum mechanics for materials engineers: the EMTO method and applications, Springer–Verlag, London, 2007.
[20] P. Soven, Coherent-potential model of substitutional disordered alloys, Phys. Rev. 156 (1967) 809.
[21] B.L. Gyorffy, Coherent-potential approximation for a nonoverlapping-muffin-tin-potential model of random substitutional alloys, Phys. Rev. B 5 (1972) 2382.
[22] J.P. Perdew, K. Burke, M. Ernzerhof, Generalized gradient approximation made simple, Phys. Rev. Lett. 77 (1996) 3865.
[23] E. Plancher, C.C. Tasan, S. Sandloebes, D. Raabe, On dislocation involvement in Ti–Nb gum metal plasticity, Scripta Mater. 68 (2013) 805.
[24] A. Devaraj, S. Nag, R. Srinivasan, R.E.A. Williams, S. Banerjee, R. Banerjee, H.L. Fraser, Experimental evidence of concurrent compositional and structural instabilities leading to ω precipitation in titanium–molybdenum alloys, Acta Mater. 60 (2012) 596.
[25] N.G. Jones, R.J. Dashwood, M. Jackson, D. Dye, β Phase decomposition in Ti–5Al–5Mo–5V–3Cr, Acta Mater. 57 (2009) 3830.
[26] S. Nag, R. Banerjee, R. Srinivasan, J.Y. Hwang, M. Harper, H.L. Fraser, Ω-Assisted nucleation and growth of α precipitates in the Ti–5Al–5Mo–5V–3Cr–0.5Fe β titanium alloy, Acta Mater. 57 (2009) 2136.
[27] F. Prima, P. Vermaut, D. Ansel, J. Debuigne, Omega precipitation in a beta metastable titanium alloy, resistometric study, Mater. Trans. 41 (2000) 1092.
[28] S. Banerjee, U.M. Naik, Plastic instability in an omega forming Ti-15% Mo alloy, Acta Mater. 44 (1996) 3667.
[29] A. Gysler, G. Lütjering, V. Gerold, Deformation behavior of age-hardened Ti–Mo alloys, Acta Metall. 22 (1974) 901.
[30] S. Hanada, M. Ozeki, O. Izumi, Deformation characteristics in β phase Ti–Nb alloys, Metall. Mater. Trans. A 16 (1985) 789.
[31] S. Hanada, O. Izumi, Transmission electron microscopic observations of mechanical twinning in metastable beta titanium alloys, Metall. Trans. A 17 (1986) 1409.
[32] Y. Hariharan, M.P. Janawadkar, T.S. Radhakrishnan, A.L.E. Terrance, G.A. Dixit, V.S. Raghunathan, Structure property correlations in superconducting Ti–Nb alloys, Pramana 26 (1986) 513.

[33] A.V. Dobromyslov, V.A. Elkin, Martensitic transformation and metastable β-phase in binary titanium alloys with d-metals of 4–6 periods, Scripta Mater. 44 (2001) 905.
[34] H.Y. Kim, Y. Ikehara, J.I. Kim, H. Hosoda, S. Miyazaki, Martensitic transformation, shape memory effect and superelasticity of Ti–Nb binary alloys, Acta Mater. 54 (2006) 2419.
[35] C.N. Reid, J.L. Routbort, R.A. Maynard, Elastic constants of Ti-40 at.% Nb at 298 K, J. Appl. Phys. 44 (1973) 1398.
[36] H.W. Jeong, Y.S. Yoo, Y.T. Lee, J.K. Park, Elastic softening behavior of Ti–Nb single crystal near martensitic transformation temperature, J. Appl. Phys. 108 (2010) 063515.
[37] L.M. Hsiung, D.H. Lassila, Shock-induced deformation twinning and omega transformation in tantalum and tantalum–tungsten alloys, Acta Mater. 48 (2000) 4851.
[38] T. Ahmed, H.J. Rack, Martensitic transformations in Ti-(16–26 at.%) Nb alloys, J. Mater. Sci. 31 (1996) 4267.